ResearchGate

See discussions, stats, and author profiles for this publication at: https://www.researchgate.net/publication/43158972

Vibrational Sum-Frequency Generation Spectroscopy at the Water/Lipid Interface: Molecular Dynamics Simulation Study

ARTICLE *in* JOURNAL OF THE AMERICAN CHEMICAL SOCIETY · MAY 2010

Impact Factor: 12.11 · DOI: 10.1021/ja100508n · Source: PubMed

CITATIONS
60

READS
32

2 AUTHORS:

Yuki Nagata
Max Planck Institute for Polymer Research
33 PUBLICATIONS **325** CITATIONS
SEE PROFILE

Shaul Mukamel
University of California, Irvine
852 PUBLICATIONS **23,722** CITATIONS
SEE PROFILE

Available from: Shaul Mukamel
Retrieved on: 29 January 2016

NIH Public Access
Author Manuscript
J Am Chem Soc. Author manuscript; available in PMC 2011 August 8.

Published in final edited form as:
J Am Chem Soc. 2010 May 12; 132(18): 6434–6442. doi:10.1021/ja100508n.

Vibrational Sum-Frequency Generation Spectroscopy at the Water/Lipid Interface: Molecular Dynamics Simulation Study

Yuki Nagata[*] and **Shaul Mukamel**[*]
University of California Irvine, Irvine, California, 92617, USA

Abstract

The sum-frequency generation (SFG) spectrum from the water/[1,2-dimyristoyl-*sn*-glycero-3-phosphatidylcholine] (DMPC) interface in the OH stretching mode region of water is simulated and shows three spectral peaks which are assigned to different environment. The weak 3590cm^{-1} peak is attributed to a few water molecules coupled to the glycerol backbone of DMCP. The 3470cm^{-1} feature comes from the top water layer adjacent to the hydrophilic head-group of DMPC. The 3290cm^{-1} peak arises from the near-bulk water nonadjacent to DMPC. The stretching mode corresponding to the 3290cm−1 peak is strongly coupled with the neighboring water molecules. In contrast, the 3470cm^{-1} mode is decoupled from the surrounding water molecules, and the orientation of water is governed by DMPC. This decoupling explains the slow relaxation dynamics of water measured in the time-resolved SFG experiment. Despite the similarity of the SFG spectra, the peak origins of water/lipid and water/vapor interfaces are different.

Introduction

A living eucaryotic cell is bounded by the plasma membrane, and the ions are actively transported to a cell cytoplasm across the membrane.[1,2] The membranes consist of the lipid bilayers, and the hydrophilic headgroups of the lipids in contact with water play an important role in the material transport. Since the structure and dynamics of water at lipid interfaces critically contribute to their stability and functionality through hydrogen-bond (H-bond) interactions,[3,4] understanding the structure and interaction between water and lipids is crucial. Considerable attention has been paid to ultrafast dynamics of water confined by reverse micelles,[5–10] at hydrophobic and hydrophilic interfaces,[11–28] and charged interfaces.[29–31] Sum-frequency generation (SFG) spectroscopy is particularly suitable for probing H-bond structures at water/lipid interfaces, because it can selectively capture the interfacial dynamics. For several lipid molecules, SFG spectra at water/lipid interfaces have two broad peaks associated with the OH stretching mode of water at 3200–3300cm^{-1} (red-shifted) and 3400–3500cm^{-1} (blue-shifted).[15,18–21,30,31] These are similar to the SFG spectra of water/vapor interfaces,[19,30] but it is not clear whether the peak assignments are the same.

Water/vapor interfaces have been extensively studied over the past 15 years. Du *et al.* attributed the blue- and red-shifted peaks to “water-like” and “ice-like” structures of interfacial water, based on the spectral similarity with bulk water and quartz-ice, respectively.[11,32] On the other hand, Sovago *et al.* used isotopic dilution and argued that these peaks were dominated by intramolecular coupling.[33] Molecular dynamics (MD) simulations have attempted to reproduce the SFG spectra and assign the peaks.[34–41] Buch assigned the blue-shifted peak to four-coordinated molecules, while the red-shifted peak was

[*]To whom correspondence should be addressed: nagatay@uci.edu; smukamel@uci.edu.

NIH-PA Author Manuscript
NIH-PA Author Manuscript
NIH-PA Author Manuscript

NIH-PA Author Manuscript

NIH-PA Author Manuscript

NIH-PA Author Manuscript

assigned to the collective excitations of intermolecularly coupled OH stretching vibrations.[38] Recently, Ishiyama and Morita successfully modelled the heterodyne-detected SFG signals[42,43] by using a MD simulation with a polarizable water model and concluded that the red-shifted peak was induced by the intermolecular orientational correlation via the anisotropic contribution of the dipole moment.[41]

In this article, we study the SFG signals at the water/lipid interface by means of a MD simulation and investigate the properties of water at the lipid interface. We used [1,2-dimyristoyl-*sn*-glycero-3-phosphatidylcholine] (DMPC) for a lipid molecule, because its force field[44] has been widely used for interpreting the X-ray data of DMPC bilayers[45] and exploring the free energy landscape at the water/DMPC interface.[28] In sec. II, we employs a truncation scheme to separate the response function into the auto- and cross-correlation parts. Section III presents the computational protocols for a MD simulation with polarizable point charges. The simulated SFG spectra are presented in Sec. IV, and the peak assignment and intermolecular couplings are discussed by using the truncated response function. Concluding remarks are given in Sec. V.

The Truncated Response Function

The SFG response function $R^{(2)}_{xxz}$ for the *s*-polarized SFG signal induced by *s*-polarized visible and *p*-polarized infrared (IR) lasers is given by[46]

$$R^{(2)}_{xxz}(t) = -\beta\langle \dot{M}_z(t) A_{xx}(0)\rangle, \tag{1}$$

where $M_z(t)$ and $A_{xx}(t)$ are the *z*-component of the total dipole moment and the *xx*-tensor of the polarizability of the system at time *t*, and $\beta = 1/kT$. Here, *z* axis and *xy* plane are perpendicular and parallel to the interface, and *s*- and *p*-polarizations denote polarizations parallel and perpendicular to the interface, respectively. The total dipole moment and polarizability are given by the sums of molecular dipole moments and polarizabilities

$$M_z(t) = \sum_i \mu_{i,z}(t), \tag{2}$$

$$A_{xx}(t) = \sum_i \alpha_{i,xx}(t), \tag{3}$$

where μ_i and α_i are the dipole moment and polarizability of molecule *i*, respectively. By inserting eqs 2 and 3 into eq 1, $R^{(2)}_{xxz}(t)$ can be separated into autocorrelation and cross-correlation terms

$$R^{(2)}_{xxz}(t) = -\beta\left\langle \sum_i \dot{\mu}_{i,z}(t)\alpha_{i,xx}(0,)\right\rangle - \beta\left\langle \sum_i \sum_{j(\neq i)} \dot{\mu}_{i,z}(t)\alpha_{j,xx}(0)\right\rangle. \tag{4}$$

The cross-correlation terms carry important information on intermolecularly correlated dynamics. They require over a few nanosecond MD trajectory for their numerical convergence, while the autocorrelation terms converge much faster.[47,48] The convergence

NIH-PA Author Manuscript

NIH-PA Author Manuscript

NIH-PA Author Manuscript

problem grows rapidly with the number of molecules N, because the number of the cross-correlation terms scales as $N(N-1)$. We introduce a computationally efficient scheme by truncating the cross-correlation terms.

Since fast intramolecular motions are spatially more localized than slow intermolecular motions, we expect the cross-correlation $\langle \mu_{i,z}\alpha_{j,xx}\rangle$ to make a small contribution to $R^{(2)}_{xxz}(t)$ for intramolecular vibrational modes when molecule i is far from molecule j. To exploit this, we define the truncated response function

$$R^{*(2)}_{xxz}(t, r_t) = -\beta\left\langle \sum_i \dot{\mu}_{i,z}(t)\alpha_{i,xx}(0)\right\rangle - \beta\left\langle \sum_i \sum_{j(\neq i)} \dot{\mu}_{i,z}(t)\alpha_{j,xx}(0) g_t(\bar{r}_{ij}.r_t)\right\rangle, \tag{5}$$

where a truncating function $g_t(r_{ij},r_t)$ depends on the truncation radius r_t and is defined by

$$g_t(r_{ij}, r_t) = \begin{cases} 1 & \text{for} \quad r_{ij} \le r_t \\ 0 & \text{for} \quad r_{ij} > r_t \end{cases}. \tag{6}$$

Note that $R^{*(2)}(t,r_t = 0)$ is the autocorrelation terms $-\beta \langle \dot{\mu}_i(t)\alpha_i(0)\rangle$, whereas $R^*(2)(t,r_t = \infty)$ is equal to $R^{(2)}(t)$. The average distance between molecules i and j, $\bar{r}_{ij} = |\bar{\mathbf{r}}_j - \bar{\mathbf{r}}_i|$, was calculated as $\bar{\mathbf{r}}_i = (1/T)\int_0^T \mathbf{r}_i(t)dt$, where T was set to be 2.4ps. Convergence of the truncated response function are accelerated for small r_t, while the accuracy increases with r_t.

Computational Protocol

Hamiltonian for MD Simulation with Polarizable Point Charges

Our model Hamiltonian is given by

$$H = K + U_{\text{intra}} + U_{\text{LJ}} + U_{\text{ele}}, \tag{7}$$

where K, U_{intra}, U_{LJ}, and U_{ele} denote the kinetic energy, intramolecular potential energy, Lennard-Jones potential energy, and electrostatic potential energy terms, respectively. In the calculations of U_{intra} and U_{LJ}, the CHARMM force field44 was used for DMPC, together with the flexible water model of Marti *et al.*.[49] The intramolecular force constant combining two H atoms of water was modified following Ref.[50]. The charge response kernel (CRK) method was used for the calculation of U_{ele} [51,52]

$$U_{\text{ele}} = \sum_i \sum_{j>i} \frac{Q_i Q_j}{4\pi\varepsilon_0} f_{1/r}(r_{ij}) - \frac{1}{2}\sum_i \sum_j V_i K_{ij} V_j, \tag{8}$$

where Q_i and V_i are the point charge and the electrostatic potential at site i, K_{ij} is the CRK combining sites i and j, and $f_{1/r}$ is the 1/r summation for the Coulomb interaction. Q and V are related to via

NIH-PA Author Manuscript

NIH-PA Author Manuscript

NIH-PA Author Manuscript

$$Q_i = Q_i^{(0)} + \Delta Q_i^{\mathrm{LF}}, \tag{9}$$

$$\Delta Q_i^{\mathrm{LF}} = \sum_j K_{ij} V_j, \tag{10}$$

$$V_i = \sum_{j(\neq i)} \frac{Q_j}{4\pi\varepsilon_0} f_{1/r}(r_{ij}), \tag{11}$$

where $Q^{(0)}$ and ΔQ^{LF} represent the gas-phase (0th order polarized) point charge and the charge induced by the local electric field, respectively. Equations (9), (10), and (11) were repeatedly solved until $\Delta Q < 0.0001e$ was achieved. For a DMPC, we used the fixed charges given by Ref.[44] and set to K=0, while we used $Q_{\mathrm{O}^1}^{(0)} = 0.6810e$, $K_{\mathrm{O}^1\mathrm{H}^2} = 3.711$a.u., and $K_{\mathrm{H}^2\mathrm{H}^3} = -0.678$a.u..[53] We multiplied K by 0.73 to avoid the divergence of the point charges in MD simulation, yielding the similar CRK parameters in Ref.[54], while the optical response was calculated without scaling. The 1–4 non-bonded interaction was included without scaling. The calculation of $f_{1/r}$ follows Ref.[53]. The Coulomb summation was calculated by using the Wolf method[55] with $\alpha = 0.1\text{Å}^{-1}$ and r_c=9.0Å.[56] To screen the short-range electrostatic interaction, the Thole's damping function[57] was introduced with the cutoffs of 2.44Å for water-water interactions[54] and 2.5Å for water-lipid interactions.

Protocol for MD Simulation

Our system consisted of 22 DMPC molecules and 1109 water molecules. The size of the prismatic unit cell was chosen to be 28.6Å in the x and y dimensions (74.4Å^2 of the surface area per a lipid molecule) and 120Å in the z dimension. Periodic boundary conditions were employed. The time step was set to be 0.4fs, and the simulated geometries were sampled every 1.2fs. The time correlation average was calculated over a single trajectory using eqs (1), (2), and (3). The molecular coordinates of the initial configuration for the DMPC/water interface were obtained from the Laboratory of Molecular & Thermodynamics Modeling at the University of Maryland.[58] We first ran a 0.3ns MD simulation for eleven independent configurations at 370K in the microcanonical ensemble and cooled the systems for 0.1ns by rescaling the velocity to reach 300K. We then equilibrated the systems in the microcanonical ensemble for 0.6ns and ran a 2ns MD simulation for sampling the snapshots.

Calculation of The Optical Response Function

We only calculated the optical response of water. The molecular dipole moment and polarizability can be decomposed into permanent and induced terms

$$\mu_i = \mu_i^{\mathrm{perm}} + \mu_i^{\mathrm{ind}}, \tag{12}$$

and

$$\alpha_i = \alpha_i^{\mathrm{perm}} + \alpha_i^{\mathrm{ind}}. \tag{13}$$

NIH-PA Author Manuscript

NIH-PA Author Manuscript

NIH-PA Author Manuscript

The molecular dipole moment for optical response function was calculated as follows. The point charges modulated by the intramolecular vibrational motion ΔQ^{vib} were calculated following Ref.[35], while the charges induced by the local electric field ΔQ^{LF} were calculated within the CRK formalism. The molecular permanent and induced dipole moments are given by

$$\mu_i^{\mathrm{perm}}=\sum_{a_i}(Q_{a_i}^{(0)}+\Delta Q_{a_i}^{\mathrm{vib}})r_{a_i}, \tag{14}$$

$$\mu_i^{\mathrm{ind}}=\sum_{a_i}\Delta Q_{a_i}^{\mathrm{LF}}r_{a_i}, \tag{15}$$

where a_i denotes the ath site in the ith molecule. For the molecular polarizability, we employed the analytical form of the permanent polarizability given by Morita and Hynes.[35] The induced polarizability was calculated via the first-order dipole-induced dipole model

$$\alpha_i^{\mathrm{ind}}=\sum_j\left(\frac{\alpha_j^{\mathrm{perm}}\alpha_i^{\mathrm{perm}}}{r_{ij}^3}-\frac{3\left(\alpha_j^{\mathrm{perm}}\mathbf{r}_{ij}\right)\cdot(\mathbf{r}_{ij}\alpha_i^{\mathrm{perm}})}{r_{ij}^5}\right)g_1(r_{ij}). \tag{16}$$

The screening function

$$g_1(r)=\begin{cases}1 & \text{for} \quad r<0.8r_c\\ 1-10x^3+15x^4-6x^5 & \text{for} \quad 0.8r_c<r<r_c\\ 0 & \text{for} \quad r_c<r\end{cases} \tag{17}$$

was used, where $x = 5r/r_c - 4$ and r_c was the same as the cutoff used in the calculation of U_{ele}.

To reduce the noise from bulk water, we introduced the screening function for the dividing surface as

$$g_{\mathrm{ds}}(z)=\mathrm{sgn}(z)\begin{cases}1 & \text{for} \quad z_{\mathrm{ds}}+a<|z|\\ \frac{1}{2}\sin\frac{\pi(z-z_{\mathrm{ds}})}{2a}+\frac{1}{2} & \text{for} \quad z_{\mathrm{ds}}-a<|z|\le z_{\mathrm{ds}}+a\\ 0 & \text{for} \quad |z|\le z_{\mathrm{ds}}-a\end{cases}, \tag{18}$$

where z_{ds} and a represented the z-coordinate of the dividing surface and the width of the screening region, respectively. By using the screening function $g_{\mathrm{ds}}(z)$, the molecular dipole moment and polarizability can be written as $\mu_i(t)g_{\mathrm{ds}}(z_i)$ and $\alpha_i(t)g_{\mathrm{ds}}^2(z_i)$, respectively. Thus, we calculated the response function

$$R_{xxz}^{*(2)}(t,r_{\mathrm{t}})=-\beta\left\langle\sum_i\dot{\mu}_{i,z}(t)\alpha_{i,xx}(0)g_{\mathrm{ds}}^3(\bar{z}_i)\right\rangle-\beta\left\langle\sum_i\sum_{j(\neq i)}\dot{\mu}_{i,z}(t)\alpha_{j,xx}(0)g_{\mathrm{t}}(\bar{r}_{ij},r_{\mathrm{t}})g_{\mathrm{ds}}(\bar{z}_i)g_{\mathrm{ds}}^2(\bar{z}_j)\right\rangle. \tag{19}$$

NIH-PA Author Manuscript

NIH-PA Author Manuscript

NIH-PA Author Manuscript

Results

Test of The Truncated Response Function

We have checked the validity of the truncated response function by simulating the linear IR response function of bulk water,

$$R_{zz}^{(1)}(t) = -\beta\langle \dot{M}_z(t) M_z(0)\rangle. \tag{20}$$

The corresponding truncated response function is given by

$$R_{zz}^{*(1)}(t, r_t) = -\beta\left\langle \sum_i \dot{\mu}_{i,z}(t)\mu_{i,z}(0)\right\rangle - \beta\left\langle \sum_i \sum_{j(\neq i)} \dot{\mu}_{i,z}(t)\mu_{j,z}(0) g_t(\bar{r}_{ij}, r_t)\right\rangle. \tag{21}$$

Our system was composed of 510 water molecules and the density was set to be 1.00 g/cm^3. The MD run was made in the microcanonical ensemble.

The IR lineshapes, $\mathrm{Im}(R_{zz}^{*(1)}(\omega, r_t))$, for various r_t are displayed in Figure 1. The peak enhanced by the cross-correlation terms in Figure 1 means that the neighboring OH stretching modes are intermolecularly coupled. The coupled OH stretching modes appears in 3200–3400cm^{-1}, which agrees with a previous study.[59] We calculated the area of the IR spectra defined by $S = (r_t)\int_{\omega_1}^{\omega_2} \mathrm{Im}(R_{zz}^{*(1)}(\omega, r_t))d\omega$ with ω_1 =3000cm^{-1} and ω_2 =3800cm^{-1}. The relative spectral areas, $S(r_t)/S(0)$, vs r_t are plotted in the inset of Figure 1. The peak enhancement stops at r_t = 4Å, and we conclude that the surrounding water molecules within a 4Å radius affects the OH stretching mode. The eigenstate associated with the OH stretching mode is estimated to be delocalized in up to 12–15 chromophores.[59,60] Since 12–15 chromophores corresponds to the number of water molecules within a ~4.4Å distance,[60] the current estimation of 4Å is in good agreement with this.

Truncating the cross-correlation terms accelerates the convergence of the response function. The MD trajectory required for the convergence of the response function can be estimated from a standard deviation of the time-domain response function

$$\sigma(t, r_t) = \left\langle \left(R_{\mathrm{snap}}^{*(1)}(t, r_t) - \left\langle R_{\mathrm{snap}}^{*(1)}(t, r_t)\right\rangle\right)^2\right\rangle, \tag{22}$$

where $R_{\mathrm{snap}}^{*(1)}(t, r_t)$ is the first-order response function for each snapshot

$$R_{zz,\mathrm{snap}}^{*(1)}(t, r_t) = -\beta\sum_i \dot{\mu}_{i,z}(t)\mu_{i,z}(0) - \beta\sum_i \sum_{j(\neq i)} \dot{\mu}_{i,z}(t)\mu_{j,z}(0) g_t(\bar{r}_{ij}, r_t), \tag{23}$$

and we have $R^{*(1)}(r, r_t) = \left\langle R_{\mathrm{snap}}^{*(1)}(t, r_t)\right\rangle$. The relative standard deviations at t=100fs, $\sigma(t$ = 100fs, $r_t)/\sigma(t$ = 100fs, r_t = 0), are presented in Figure 2. When r_r is small, the fluctuation of the response function decreases, and the required trajectory for convergence of the response function becomes shorter. In the coming sections, we use the truncated response function for surveying the intermolecular couplings of the OH stretching modes in the SFG signals.

NIH-PA Author Manuscript

NIH-PA Author Manuscript

NIH-PA Author Manuscript

SFG Spectra of the Water/DMPC Interface

A snapshot of a simulated water/DMPC system is shown in Figure 3, along with the profiles of the density and *z*-component of the dipole moment of water. The average dipole at the water/lipid interface had a maximum of 0.51 Debye for an area/molecule of 74.4Å^2 and is much larger than that reported for the water/vapor interface.[41] The strong Coulomb interaction between the hydrophilic headgroup of DMPC and water influences the orientation of the water molecules. Since the intensity of the *ssp* SFG spectra depends on the *z*-component of the dipole moment, the SFG spectra are expected to be stronger at the water/lipid interface than at the water/vapor interface. This is consistent with, for example, Figure 2 of Ref.[19]. The dipole profile shows an interesting feature; water molecules tend to orient with respect to DMPC when they move from the bulk to the Gibbs dividing surface (12Å≤ $|z|$ ≤17Å), and their orientations are randomized when they move towards the lipid layer (17Å≤ $|z|$ ≤22Å). These features are in good agreement with a previous Monte Carlo simulation.[26]

The density and dipole profiles in Figure 3 imply that water orients in random directions for the region of $|z|$ ≤12Å and shall make no contribution to the SFG signal. We, thus, set the dividing surface as r_{ds}=12Å and a=1Å. The truncation radius was set to r_t = 9Å. Note that $R^{(2)}_{xxz}(t)$ did not fully converge with a 22ns MD trajectory was used. The simulated SFG spectra are shown in Figure 4. It is reasonable to compare with the experimental SFG spectrum at the water/[1,2-dipalmitoyl-*sn*-glycero-3-phosphocholine] (DPPC) interface,[21] since DPPC and DMPC have the same hydrophilic headgroup and glycerol backbone. The simulated $|R^{*(2)}_{xxz}(\omega)|^2$ have two peaks at 3250 and 3480cm^{-1}, while the frequencies of the peaks at the experimental SFG spectrum are estimated to be 3280 and 3430cm^{-1} from Figure 2(b) of Ref.[21]. The full width of half maximum (FWHM) of the 3250cm^{-1} peak in the simulated $|R^{*(2)}_{xxz}(\omega)|^2$ was 214cm^{-1}, while the FWHM of the experimental SFG spectrum are estimated to be 200cm^{-1}.[21] Our simulation reproduced the overall experimental spectral shapes with slight frequency shifts. Note that the water model employed here contains both the symmetric and anti-symmetric modes,[49] which are not resolved due to the large broadening.

In Figure 4, the imaginary part of the SFG response function is positive, indicating that the water dipole moments at the water/DMPC interface point towards the lipid layer. Water orienting toward the DMPC layer can also be seen in the dipole profile of Figure 3 and in the angle profile between the lipid normal vector and water dipole in Figure 1 of Ref.[26]. However, the imaginary part of the SFG spectrum fitted by using the maximum entropy method (MEM)[61] showed two negative peaks at the D_2O/DPPC interface, indicating that interfacial water oriented not to the interface but to the bulk.[31] The current MD simulation as well as a previous Monte Carlo simulation[26] seem to be at variance with the fit obtained by using the MEM.[31] In the MEM, however, the difference between two positive peaks and two negative peaks in $\mathrm{Im}(R^{(2)}_{xxz}(\omega))$ appears only in the sign of the MEM phase, which cannot be determined uniquely from the power spectrum $|R^{(2)}_{xxz}(\omega)|^2$. Thus, the phase-sensitive (heterodyne-detected) SFG experiments[30,42,62,63] are required to reveal the water orientation at the water/DMPC or water/DPPC interfaces.

Identification of Surface and Bulk Contributions

To investigate how interfacial water at various depths contributes to the SFG signal, we computed the SFG spectra by moving the dividing surface. These are shown in Figure 5. The spectrum for z_{ds}=19Å shows one peak at 3590cm^{-1}, while for z_{ds}=12Å we observed two major peaks at 3290cm^{-1} (red-shifted) and 3470cm^{-1} (blue-shifted). Here, two

NIH-PA Author Manuscript

NIH-PA Author Manuscript

NIH-PA Author Manuscript

interpretations for the peak assignments might be possible. One assumes that the red-shifted peak position is invariant, while the blue-shifted peak is continuously red-shifted with the dividing surface. The other interpretation is that three peaks are present and the peak positions are stationary. A weak ~3600cm^{-1} peak has been observed in the pump-probe signals of several low hydrated lipid systems (1-palmitoyl-2-linoleyl-phosphatidylcholine (PLPC),[22] 1,2-dilauroyl-*sn*-glycero-3-phosphocholine (DLPC),[25] and 1-palmitoyl-2-oleoylphosphatidylcholine (POPC)[64]). Thus, we adopt the latter interpretation.

The peak areas for various depths of the dividing surface calculated by fitting the SFG spectra with three Gaussians that have the peaks at 3290, 3470, and 3590cm^{-1} are displayed in Figure 6. The area of the 3590cm^{-1} peak is unchanged as the dividing surface is moved from the lipid bilayer to the bulk, indicating that the 3590cm^{-1} peak arises mainly from water in the region of $|z| \geq 19$Å (region I). In contrast, the spectral areas for the red- and blue-shifted peaks do not contribute to the SFG spectra for z_{ds}=19Å and increase as the dividing surface is moved toward the bulk. The spectral area of the blue-shifted peak increases linearly with the dividing surface in the range of 15Å≤ $|z|$ ≤19Å (region II), and the increase in the spectral area is saturated for 12Å≤ $|z|$ ≤15Å (region III). The red-shifted peak, in contrast, increases in region III.

Correlations with Neighboring Molecules

Intermolecular coupling of interfacial water shows up in the SFG spectra mainly through the cross-correlation terms in the response function. Variation of the signals with the truncation radius r_t reveals the strength of the intermolecular dynamical correlation, as discussed above. Since the water/lipid interface is anisotropic, we employed two types of ellipsoidal truncations instead of the spherical truncation given by eq 6. The parallel truncations in which $R^{*(2)}_{xxz}(t, r_t)$ included the cross-correlation parallel to the interface is defined as

$$g_t(r)=\begin{cases} 1 & \text{for } \left(\frac{r_{ij(x)}}{r_t}\right)^2+\left(\frac{r_{ij(y)}}{r_t}\right)^2+\left(\frac{r_{ij(z)}}{b}\right)^2 \leq 1 \\ 0 & \text{for } \left(\frac{r_{ij(x)}}{r_t}\right)^2+\left(\frac{r_{ij(y)}}{r_t}\right)^2+\left(\frac{r_{ij(z)}}{b}\right)^2 > 1 \end{cases}, \tag{24}$$

whereas the perpendicular truncation in which $R^{*(2)}_{xxz}(t, r_t)$ included the cross-correlation perpendicular to the interface (Figure 7) is defined as

$$g_t(r)=\begin{cases} 1 & \text{for } \left(\frac{r_{ij(x)}}{b}\right)^2+\left(\frac{r_{ij(y)}}{b}\right)^2+\left(\frac{r_{ij(z)}}{r_t}\right)^2 \leq 1 \\ 0 & \text{for } \left(\frac{r_{ij(x)}}{b}\right)^2+\left(\frac{r_{ij(y)}}{b}\right)^2+\left(\frac{r_{ij(z)}}{r_t}\right)^2 > 1 \end{cases}, \tag{25}$$

where b denotes the constant radius of the ellipsoidal bodies and we set to b = 2Å. Simulated SFG spectra with the parallel and perpendicular truncations are shown in Figure 8. In both truncations, the cross-correlation terms made a small contribution to the blue-shifted peak, while the red-shifted peak grows with r_t. These indicate that the OH stretching mode corresponding to the blue-shifted peak is not coupled with the neighboring water molecules, while the OH stretching mode for the red-shifted peak is coupled with.

For an in-depth analysis of the contribution of the cross-correlation terms to the SFG spectra, the spectral areas for various r_t, $S(r_t)$, were calculated for the red- and blue-shifted peaks by fit-ting three Gaussians to $\mathrm{Im}(R^{*(2)}_{xxz}(\omega, r_t))$ in the region 3000cm^{-1} ≤ ω ≤3800cm^{-1}. The relative SFG spectral areas, $S(r_t)/S(0)$, vs r_t are plotted in Figure 9 with the IR spectral

NIH-PA Author Manuscript

NIH-PA Author Manuscript

NIH-PA Author Manuscript

area for bulk water. Weak cross-correlation of the blue-shifted peak implies that the OH stretching modes are not coupled with the neighboring water molecules unlike in bulk water. In particular, the small but negative cross-correlation in Figure 9(b) means that the neighboring water dipole moments orient in opposite directions, because the sign of the *ssp* SFG signal is determined by the water orientation. This can be related to the following microscopic picture: DMPC is positively charged around the N atom and negatively charged around the P atom. Near the negatively charged part, the water dipole moments orient to DMPC, while they orient against DMPC near the positively charged part, giving rise to the opposite orientations of the neighboring water molecules. These opposite orientations of the neighboring water molecules cause the repulsive dipole-dipole interaction. The top-layer water adjacent to DMPC stabilizes the water/DMPC interface by minimizing the interaction energy between water and DMPC at the expense of the repulsive dipole-dipole interactions between neighboring water molecules. These findings indicate that the orientation of water is governed by the hydrophilic headgroup of DMPC rather than the surrounding water.

The red-shifted peak contains a much larger contribution from the cross-correlation terms than the blue-shifted peak in Figure 9, indicating that the OH stretching modes associated with the red-shifted peak are intermolecularly coupled with those of the neighboring water molecules. In particular, the cross-correlation in the perpendicular direction is larger than in the parallel direction, indicating that the strength of the intermolecular coupling is anisotropic. The electrostatic interaction between the hydrophilic headgroup of DMPC and water makes not only the ordered structure of water but also the anisotropic coupling of the OH stretching mode.

Peak Assignments

The 3590cm^{-1} peak has the largest intensity when the SFG spectra for region I of the density profile (Figure 3) was extracted by setting the dividing surface at z_{ds}=19Å, while the peak was not enhanced when the dividing surface was moved toward the bulk in contrast with the other two peaks (Figure 5 and Figure 6). The water density profile indicates that in region I water is less dense and is surrounded by DMPC. The typical snapshot of water corresponding to this peak is denoted in the blue circle of Figure 10. As depicted in this figure, this high OH stretch frequency arises from the coupling with the glycerol backbone of DMPC. Binder assigned this peak to clusters of a few waters with two or fewer H-bonds each,[64] whereas Zhao *et al.* ascribed it to water in the hydrophobic region of the lipid layer.[25] The present analysis using the dividing surface and the snapshot of the MD simulation suggests that the 3590cm^{-1} peak comes from a few water molecules coupled to the glycerol backbone of DMPC. This peak was, however, much weaker than the other two peaks in the SFG spectra.

The spectral intensity of the blue-shifted (3470cm^{-1}) peak was increased in region II of the density profile when the dividing surface was moved toward the bulk (Figure 5 and Figure 6). Figure 3 shows that in region II water density increases with the dividing surface, and water makes a layer. The cross-correlation makes a small contribution to the SFG spectra in Figure 8 and Figure 9, indicating that the OH stretching modes corresponding to this peak are not intermolecularly coupled with those of the neighboring water molecules. This implies that the OH stretching mode is coupled to the hydrophilic headgroup of DMPC rather than the surrounding water. The typical snapshot of water corresponding to this peak is denoted in the red circle of Figure 10.

The red-shifted (3290cm^{-1}) peak is enhanced in both regions II and III of the density profile. Figure 3 shows that water occupies most of the space in region III, and the near-bulk water nonadjacent to DMPC is dominant. In Figure 8 and Figure 9, the cross-correlation terms contribute to the SFG signals in contrast with the blue-shifted peak, which indicates

NIH-PA Author Manuscript

NIH-PA Author Manuscript

NIH-PA Author Manuscript

that the OH stretching modes associated with the red-shifted peak are coupled with those of the neighboring water molecules. A typical snapshot of water corresponding to this peak is denoted in the green circle of Figure 10.

For the low hydrated phospholipids, the peak appears at 3420cm^{-1} in the two-dimensional (2D) IR signal[22] and 3380cm^{-1} in the pump-probe experiment.[25] Since the simulated frequency was higher by 50cm^{-1} than the experimental SFG signal[21] for the blue-shifted peak, the peak measured at 3380–3420cm^{-1} should correspond to the blue-shifted peak. Volkov *et al.* showed that in the low hydrated phospholipid, most of the water molecules formed H-bonds with DMPC.[24] Thus, we can expect that the top-layer water adjacent to DMPC, thus, contributes to the blue-shifted peak. This is consistent with the current study.

Concluding Remarks

We have employed a MD simulation with polarizable point charges to compute the SFG spectra for the water OH stretching mode and found three peaks at 3590, 3470 (blue-shifted), and 3290cm^{-1} (red-shifted). The 3590cm^{-1} peak is very weak in the SFG spectra (Figure 5), although it has been observed in IR spectra of the low hydrated lipid systems.[22,25,64] The water density profile in Figure 3 and the snapshot in Figure 10 shows that a few water molecules coupled to the glycerol backbone of DMPC contribute to this peak.

The imaginary parts of the blue- and red-shifted peaks are positive, indicating that the water dipole moments associated with these modes point from the bulk to the lipid layer. The fitted spectra have negative peaks for both modes.[31] Heterodyne-detected SFG experiments[30,42,62,63] are required to get the signs of $\mathrm{Im}(R^{(2)}_{xxz})$ at the water/DMPC interface. We assigned the blue- and red-shifted peaks to water adjacent and nonadjacent to the hydrophilic headgroups of DMPC, respectively. The analysis based on the truncated response function shows that the cross-correlation terms of the response function $\langle \mu_{j,z}\alpha_{i,xx}\rangle$ make a much weaker contribution to the blue-shifted peak than to the red-shifted peak. The large cross-correlation associated with the red-shifted peak indicates the OH stretching modes are coupled with the OH stretching modes of neighboring water, while the small cross-correlation associated with the blue-shifted peak indicates the weak intermolecular couplings. For the blue-shifted peak, the orientation of water and the intermolecular coupling of the OH stretching mode are governed by DMPC rather than the surrounding water molecules.

At the water/vapor interface, the blue- (~ 3400cm^{-1}) and the red-shifted (~ 3200cm^{-1}) peaks have been assigned to the near-bulk and top-layer water, respectively.[43,66] In contrast, we showed that the blue- and red-shifted peaks come from the top-layer water adjacent to DMPC, and the near-bulk water nonadjacent to DMPC at the water/DMPC interface. Although the SFG spectra of the water/vapor and water/lipid interfaces are similar,[19,30] the peak origins are different.

Finally, we comment on the relaxation of the water OH stretching mode at the vapor and the lipid interfaces. The time-resolved SFG spectroscopy showed that water corresponding to the blue-shifted peak had the rapid relaxation of the OH stretching mode, whereas water corresponding to the red-shifted peak had the slow relaxation. The relaxation time for the red-shifted mode was estimated to ~150fs[65] and ~200fs,[19,67] which was compatible to the relaxation time in the bulk water.[68] In contrast, at the water/lipid interface, the red- and blue-shifted OH stretching modes show the rapid (~100fs) and slow (~500fs) relaxations, respectively.[18] The present study indicates that the lack of intermolecular coupling between the OH stretching modes causes the slow relaxation for water corresponding to the blue-

NIH-PA Author Manuscript

NIH-PA Author Manuscript

NIH-PA Author Manuscript

shifted peak, whereas the strong intermolecular couplings accelerate the relaxation for the red-shifted peak.

Future MD simulations will focus on the surface-specific 2D spectra with an even-order susceptibility.[69,70] Possible pulse configurations for surface-specific 2D are IR-IR-IR ($\chi^{(2)}$) and IR-IR-IR-Visible ($\chi^{(4)}$). Ultrafast 2D vibrational spectroscopy can capture information on the intermode coupling and inhomogeneity of liquid dynamics.[71–74] We had proposed 2D IR surface spectroscopy for detecting the interadsorbate coupling on metal surface by using the IR-IR-IR pulse configuration.[70] Cheon *et al.* pointed out that the 2D technique with the even-order susceptibility carries information on the chiral couplings.[75] The surface-specific 2D experiment was conducted on the model membrane system by using the IR-IR-IR-Visible pulse configuration.[76,77] The applications of these surface-specific 2D techniques to the water/lipid interface will provide a new experimental tool for probing the information on the intermolecular coupling of interfacial water.

Acknowledgments

We wish to thank Prof. Y. R. Shen for fruitful discussion. The supports of the National Institutes of Health (Grant No. GM-59230) and the National Science Foundation (Grant No. CHE-0745892) are gratefully acknowledged.

References

1. Carafoli E. Physiolog Rev. 1991; 71:129–153.
2. Toyoshima C. Arch Biochem Biophys. 2008; 476:3–11. [PubMed: 18455499]
3. Lindahl E, Sansom MSP. Curr Opin Struct Biol. 2008; 18:425–431. [PubMed: 18406600]
4. Sotomayor CP, Aguilar LF, Cuevas FJ, Helms MK, Jameson DM. Biochem. 2000; 39:10928–10935. [PubMed: 10978181]
5. Shirota H, Horie K. J Phys Chem B. 1999; 103:1437–1443.
6. Dokter AM, Woutersen S, Bakker HJ. J Chem Phys. 2007; 126:124507. [PubMed: 17411144]
7. Moilanen DE, Levinger NE, Spry DB, Fayer MD. J Am Chem Soc. 2007; 46:14311–14318. [PubMed: 17958424]
8. Balakrishnan S, Javid N, Weigartner H, Winter R. Chemphyschem. 2008; 9:2794–2801. 2008. [PubMed: 19016296]
9. Pieniazek PA, Lin YS, Chowdhary J, Ladanyi BM, Skinner JL. J Phys Chem B. 2009; 113:15017–15028. [PubMed: 19842648]
10. Chowdhary J, Ladanyi BM. J Phys Chem B. 2009; 113:15029–15039. [PubMed: 19842706]
11. Du Q, Freysz E, Shen YR. Science. 1994; 264:826–828. [PubMed: 17794723]
12. Scatena LF, Brown MG, Richmond GL. Science. 2001; 292:908–912. [PubMed: 11340199]
13. Richmond GL. Chem Rev. 2002; 102:2693–2724. [PubMed: 12175265]
14. Moore FG, Richmond GL. Acc Chem Res. 2008; 41:739–748.
15. Tyrode E, Johnson CM, Kumpulainen A, Rutland MW, Claesson PM. J Am Chem Soc. 2005; 127:16848–16859. [PubMed: 16316231]
16. Liu WT, Zhang L, Shen YR. J Chem Phys. 2006; 125:14711.
17. Zhang L, Singh S, Tian C, Shen YR, Wu Y, Shannon MA, Brinker CJ. J Chem Phys. 2009; 130:154702. [PubMed: 19388765]
18. Ghosh A, Smits M, Bredenbeck J, Bonn M. J Am Chem Soc. 2007; 129:9608, 2007. [PubMed: 17637056]
19. Ghosh A, Smits M, Sovago M, Bredenbeck J, Muller M, Bonn M. Chem Phys. 2008; 350:23–30.
20. Eftekhari-Bafrooei A, Borguet E. J Am Chem Soc. 2009; 131:12034. [PubMed: 19663486]
21. Viswanath P, Aroti A, Motschmann H, Leontidis E. J Phys Chem B. 2009; 113:14816–14823. [PubMed: 19824633]
22. Volkov VV, Palmer DJ, Righini R. Phys Rev Lett. 2007; 99:078302, 2007. [PubMed: 17930929]

NIH-PA Author Manuscript

NIH-PA Author Manuscript

NIH-PA Author Manuscript

23. Volkov VV, Palmer DJ, Righini R. J Phys Chem B. 2007; 111:1377–1383. [PubMed: 17249718]
24. Volkov VV, Takaoka Y, Righini R. J Phys Chem B. 2009; 113:4119–4124. [PubMed: 19228033]
25. Zhao W, Moilanen DE, Fenn EE, Fayer MD. J Am Chem Soc. 2008; 130:13927–13937. [PubMed: 18823116]
26. Jedlovszky P, Mezei M. J Phys Chem B. 2001; 105:3614–3623.
27. Brown MG, Walker DS, Raymond A, Richmond GL. J Phys Chem B. 2003; 107:237–244.
28. Matubayasi N, Shinoda W, Nakahara M. J Chem Phys. 2008; 128:195107. [PubMed: 18500905]
29. Tian CS, Shen YR. Proc Natl Acad Sci USA. 2009; 106:15148–15153. [PubMed: 19706483]
30. Nihonyanagi S, Yamaguchi S, Tahara T. J Chem Phys. 2009; 130:204704. [PubMed: 19485472]
31. Sovago M, Vartiainen E, Bonn M. J Chem Phys. 2009; 131:161107. [PubMed: 19894919]
32. Du Q, Superfine R, Freysz E, Shen YR. Phys Rev Lett. 1993; 70:2313–2316. [PubMed: 10053529]
33. Sovago M, Campen RK, Wurpel GWH, Muller M, Bakker HJ, Bonn M. Phys Rev Lett. 2008; 100:173901. [PubMed: 18518288]
34. Morita A, Hynes JT. Chem Phys. 2000; 258:371–390.
35. Morita A, Hynes JT. J Phys Chem B. 2002; 106:673–685.
36. Perry A, Ahlborn H, Space B, Moore PB. J Chem Phys. 2003; 118:8411–8419.
37. Brown EC, Mucha M, Jungwirth P, Tobias DJ. J Phys Chem B. 2005; 109:7934–7940. [PubMed: 16851926]
38. Buch V. J Phys Chem B. 2005; 109:17771–17774. [PubMed: 16853275]
39. Perry A, Neipert C, Space B, Moore PB. Chem Rev. 2006; 106:1234–1258. [PubMed: 16608179]
40. Auer BM, Skinner JL. J Phys Chem B. 2009; 113:4125–4130. [PubMed: 19425249]
41. Ishiyama T, Morita A. J Phys Chem C. 2009; 113:16299–16302.
42. Ji N, Ostroverkhov V, Tian CS, Shen YR. Phys Rev Lett. 2008; 100:096102. [PubMed: 18352727]
43. Tian CS, Shen YR. J Am Chem Soc. 2009; 131:2790. [PubMed: 19209852]
44. Klauda JB, Brooks BR, MacKerell AD, Venable RM, Pastor RW. J Phys Chem B. 2005; 109:5300–5311. [PubMed: 16863197]
45. Klauda JB, Kucerka N, Brooks BR, Pastor PW, Nagle JF. Biophys J. 2006; 90:2796–2807. [PubMed: 16443652]
46. Mukamel, S. Principles of Nonlinear Optical Spectroscopy. Oxford University Press; New York: 1995.
47. Gaigeot MP, Sprik M. J Phys Chem B. 2003; 107:10344–10358.
48. Gaigeot MP, Vuilleumeier R, Sprik M, Borgis D. J Chem Theory Comput. 2005; 1:772–789.
49. Marti J, Padro JA, Guardia E. J Mol Liq. 1994; 62:17–31.
50. Ishiyama T, Morita A. J Phys Chem C. 2007; 111:721–737.
51. Morita A, Kato S. J Am Chem Soc. 1997; 119:4021–4032.
52. Morita A, Kato S. J Chem Phys. 1998; 108:6809–6818.
53. Nagata Y. Chemphyschem. 2010; 11:474–479. [PubMed: 19998311]
54. Iuchi S, Morita A, Kato S. J Phys Chem B. 2002; 106:3466–3476.
55. Wolf D, Keblinski P, Phillpot SR, Eggebrecht J. J Chem Phys. 1999; 110:8254–8282.
56. Fennell CJ, Gezelter JD. J Chem Phys. 2006; 124:234104. [PubMed: 16821904]
57. Thole BT. Chem Phys. 1981; 59:341–350.
58. http://terpconnect.umd.edu/jbklauda/research/download.html
59. Auer BM, Skinner JL. J Chem Phys. 2008; 128:224511. [PubMed: 18554033]
60. Kraemer D, Cowan ML, Paarman A, Huse N, Nibbering ETJ, Elsaesser T, Miller RJD. Proc Natl Acad Sci USA. 2008; 105:437–442. [PubMed: 18182497]
61. Sovago M, Vartiainen E, Bonn M. J Phys Chem C. 2009; 113:6100–6106.
62. Ostroverkhov V, Waychunas GA, Shen YR. Phys Rev Lett. 2005; 94:046102. [PubMed: 15783575]
63. Stiopkin IV, Jayathilake HD, Bordenyuk AN, Benderskii AV. J Am Chem Soc. 2008; 130:2271–2275. [PubMed: 18217755]

NIH-PA Author Manuscript

NIH-PA Author Manuscript

NIH-PA Author Manuscript

64. Binder H. Eur Biophys J. 2007; 36:265–279. [PubMed: 17089150]
65. McGuire JA, Shen YR. Science. 2006; 313:1945–1948. [PubMed: 17008527]
66. Fan Y, Chen X, Yang L, Cremer PS, Gao YQ. J Phys Chem B. 2009; 113:11672–11679. [PubMed: 19653670]
67. Smits M, Ghosh A, Sterrer M, Muller M, Bonn M. Phys Rev Lett. 2007; 98:098302. [PubMed: 17359206]
68. Cowan ML, Bruner BD, Huse N, Dwyer JR, Chugh B, Nibbering ETJ, Elsaesser T, Miller RJD. Nature. 2005; 434:199–202. [PubMed: 15758995]
69. Cho MH. J Chem Phys. 2000; 112:9978–9985.
70. Nagata Y, Tanimura Y, Mukamel S. J Chem Phys. 2007; 126:204703. [PubMed: 17552785]
71. Mukamel S, Abramavicius D, Yang L, Zhuang W, Schweigert IV, Voronine V. Acc Chem Res. 2009; 42:553. [PubMed: 19323494]
72. Yagasaki T, Saito S. Acc Chem Res. 2009; 42:1250–1258. [PubMed: 19469530]
73. Tanimura Y, Ishizaki A. Acc Chem Res. 2009; 42:1270–1279. [PubMed: 19441802]
74. Jeon J, Yang S, Choi JH, Cho M. Acc Chem Res. 2009; 42:1280–1289. [PubMed: 19456096]
75. Cheon S, Lee H, Choi JH, Cho MH. J Chem Phys. 2007; 126:054505. [PubMed: 17302483]
76. Bredenbeck J, Ghosh A, Smits M, Bonn M. J Am Chem Soc. 2008; 130:2152. [PubMed: 18225904]
77. Bredenbeck J, Ghosh A, Nienhuys HK, Bonn M. Acc Chem Res. 2009; 42:1332–1342. [PubMed: 19441810]

NIH-PA Author Manuscript

NIH-PA Author Manuscript

NIH-PA Author Manuscript

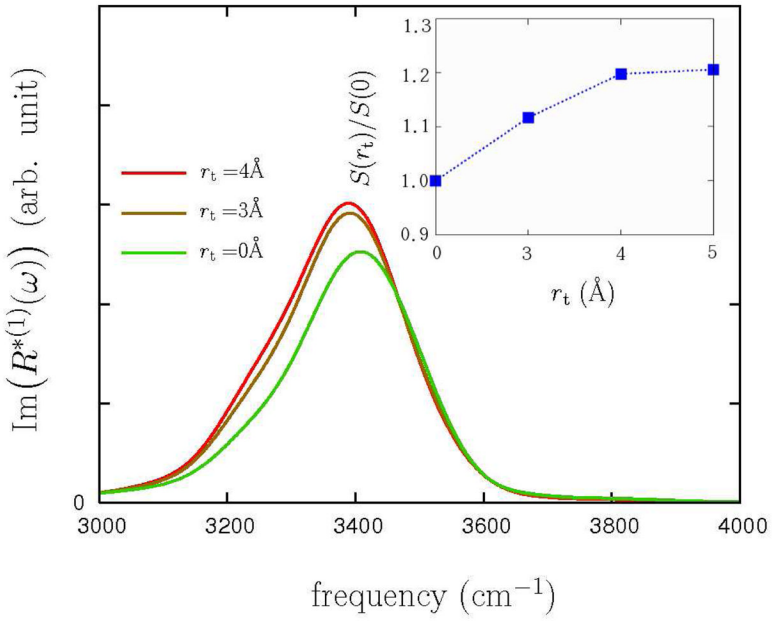

Figure 1.

Simulated IR spectra, $\mathrm{Im}(R^{*(1)}_{zz}(\omega, r_t))$, of bulk water for various truncation radii. Inset: Relative areas of the IR spectra, $S(r_t)/S(0)$, vs the truncation radius r_t.

NIH-PA Author Manuscript

NIH-PA Author Manuscript

NIH-PA Author Manuscript

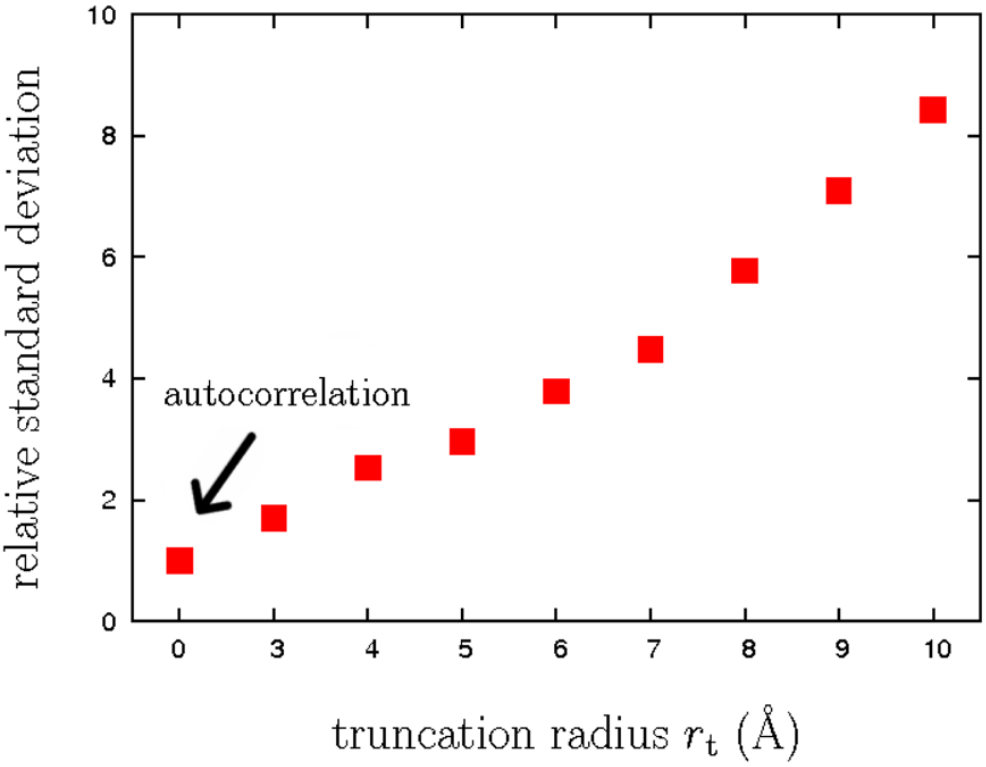

Figure 2.

Variation of the relative standard deviations of $R_{zz}^{*(1)}(t, r_t)$ at t=100fs, σ(t = 100fs,r_t)/σ(t = 100fs,r_t = 0) with the truncation radius r_t.

NIH-PA Author Manuscript

NIH-PA Author Manuscript

NIH-PA Author Manuscript

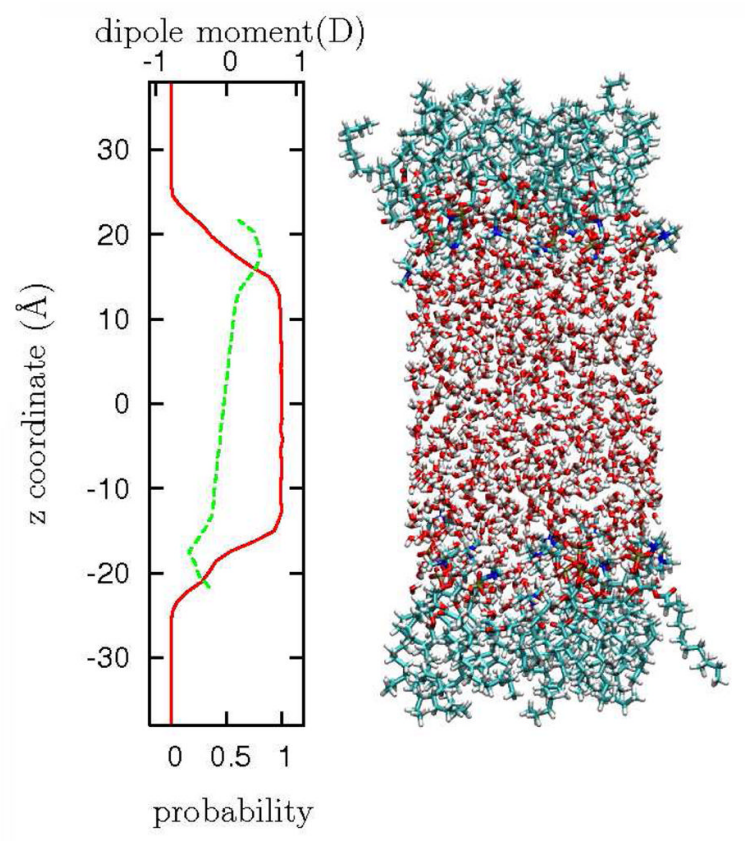

Figure 3.
Left: Density profile (solid line) and profile of the *z*-component of dipole moment per water molecule (broken line). Right: Snapshot of the simulated water/DMPC interface. Water and DMPC molecules are denoted in red and green colors.

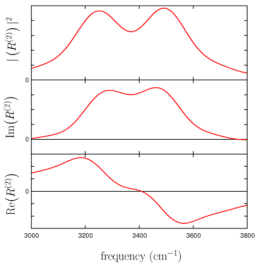

Figure 4.

Simulated SFG spectra of the water/DMPC interface, $|R^{*(2)}_{xxz}(\omega, r_t=9\text{Å})|^2$, $\mathrm{Im}(R^{*(2)}_{xxz}(\omega, r_t=9\text{Å}))$, and $\mathrm{Re}(R^{*(2)}_{xxz}(\omega, r_t=9\text{Å}))$. Arbitrary units are used.

NIH-PA Author Manuscript NIH-PA Author Manuscript NIH-PA Author Manuscript

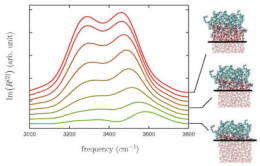

Figure 5.

Simulated SFG spectra, $\mathrm{Im}(R^{*(2)}_{xxz}(\omega, r_t=9\text{Å}))$, for various depths of the dividing surfaces. From top to bottom, z_{ds}=12, 13, 14, 15, 16, 17, 18, and 19Å.

NIH-PA Author Manuscript
NIH-PA Author Manuscript
NIH-PA Author Manuscript

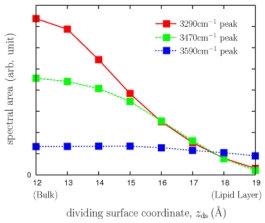

Figure 6.
Areas of the 3290, 3470, and 3590cm^{-1} peaks for various dividing surfaces. Lines are guide for eyes.

NIH-PA Author Manuscript
NIH-PA Author Manuscript
NIH-PA Author Manuscript

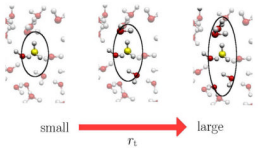

Figure 7.
Schematic picture of the perpendicular truncation of the cross-correlation terms (eq 25). The truncation parameter r_t is increased from left to right.

NIH-PA Author Manuscript
NIH-PA Author Manuscript
NIH-PA Author Manuscript

NIH-PA Author Manuscript
NIH-PA Author Manuscript
NIH-PA Author Manuscript

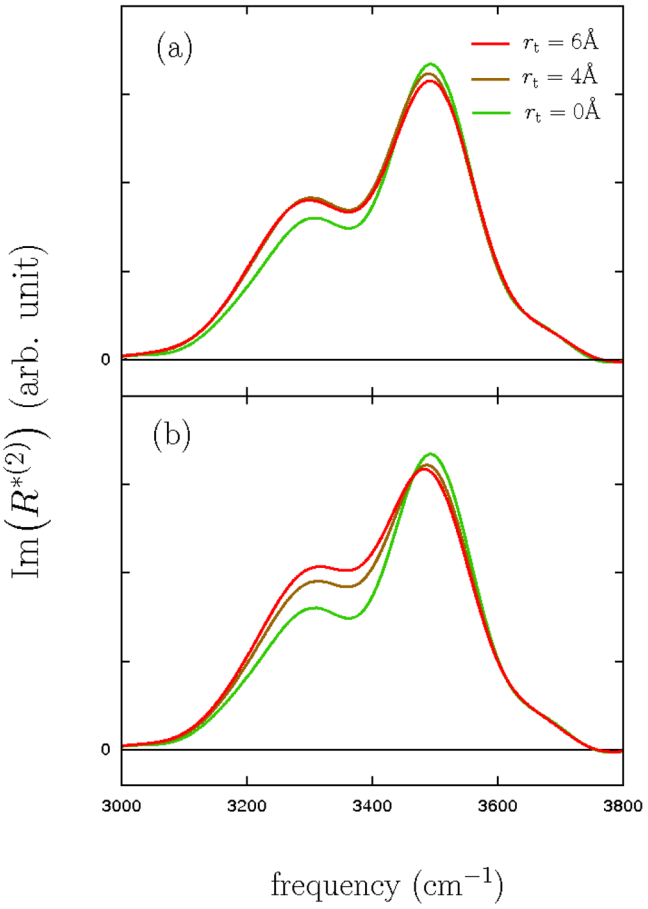

Figure 8.

Simulated SFG spectra, $\mathrm{Im}(R^{*(2)}_{xxz}(\omega, r_t))$, for (a) parallel truncation (eq 24) and (b) perpendicular truncation (eq 25).

NIH-PA Author Manuscript

NIH-PA Author Manuscript

NIH-PA Author Manuscript

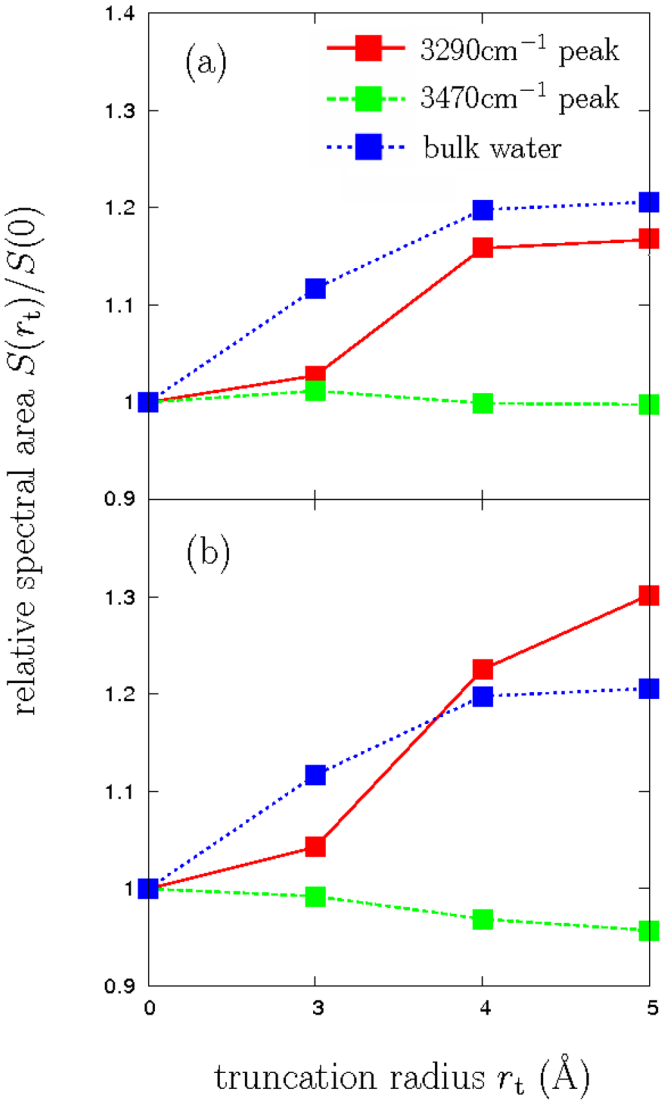

Figure 9.
Relative areas, $S(r_t)/S(0)$, of interfacial water corresponding to the red- and blue-shifted peaks for (a) parallel truncation (eq 24) and (b) perpendicular truncation (eq 25). Relative areas of bulk water is also shown for comparison.(see Inset of Figure 1.)

NIH-PA Author Manuscript

NIH-PA Author Manuscript

NIH-PA Author Manuscript

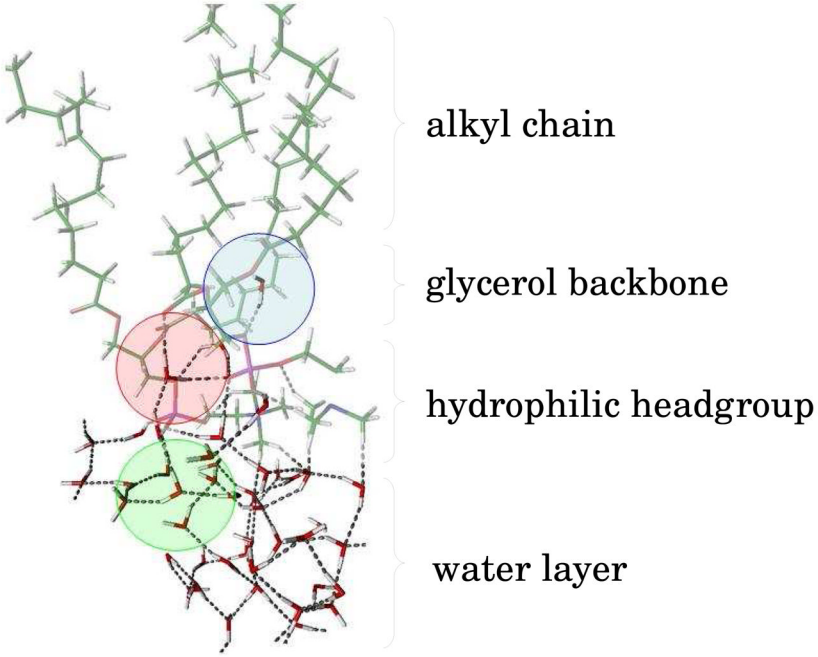

Figure 10.
Snapshot of the water/DMPC. Water molecules corresponding to 3590, 3470, 3290cm^{-1} peaks are highlighted in the blue, red, and green circles, respectively. The dashed lines represent the H-bonds.